

# A Method for Controlling Sensitivity of Fabry–Perot Interferometer Sensors Based on Vernier Effect



Le-yi Hou, Ben Xu, and Chun-liu Zhao

**Abstract** Optical fiber cascaded Fabry–Perot interferometers temperature sensors based on Vernier effect are studied in detail by theoretical simulation. The simulation results show that the free spectrum range (FSR) difference of the two Fabry–Perot interferometers affects the temperature sensitivity. When the value of the FSR difference is positive, the temperature sensitivity is positive too. Otherwise, the temperature sensitivity is negative. Furthermore, the temperature sensitivity of the Fabry–Perot interferometer sensors based on Vernier effect is higher with the FSR difference smaller. Therefore, we propose a method for controlling the sensitivity of the Fabry–Perot interferometer sensors based on Vernier effect by adjusting the difference of the two FSR.

**Keywords** Cascaded Fabry–Perot interferometers · Vernier effect · Temperature sensitivity · Free spectrum range difference

## 1 Introduction

Fabry–Perot interferometer (FPI) is universally developed and employed in pressure sensing [1, 2], strain sensing [3], temperature sensing [2], hydrogen sensing [4] and refractive index sensing [5, 6] field own to good performance as well as simple in construct. Recent years, optical Vernier effect has been attracted great interesting because which can improve sensitivity greatly [7, 8]. Especially FPI sensors based on Vernier effect are fabricated and applied to the enlargement of sensing sensitivity universally [4, 9, 10]. However, we notice that the temperature sensitivity of the

---

L. Hou · B. Xu · C. Zhao (✉)

Institute of Optoelectronic Technology, Jiliang University China, Hangzhou, China

e-mail: [clzhao@cjlu.edu.cn](mailto:clzhao@cjlu.edu.cn); [zhchunliu@hotmail.com](mailto:zhchunliu@hotmail.com)

L. Hou

e-mail: [190996854@qq.com](mailto:190996854@qq.com)

B. Xu

e-mail: [xuben@cjlu.edu.cn](mailto:xuben@cjlu.edu.cn)

© Springer Nature Singapore Pte Ltd. 2021

L. Xu and L. Zhou (eds.), *Proceedings of the 8th International Multidisciplinary*

*Conference on Optofluidics (IMCO 2018)*, Lecture Notes in Electrical Engineering 531,

[https://doi.org/10.1007/978-981-13-3381-1\\_1](https://doi.org/10.1007/978-981-13-3381-1_1)

FPI sensors based on Vernier effect has different characteristics. Sometimes, the sensitivity of the FPI sensor based on Vernier effect is positive, and sometimes that is negative. Moreover, the values of the sensitivity are various from the length of the FPIs' cavities. Almost no one has found it and made a clear explanation for the phenomenon.

In this paper, optical fiber cascaded Fabry–Perot interferometers (CFPIs) sensors based on Vernier effect are studied by simulation. Results indicate that Vernier effect appears in the CFPIs sensors with the length of the HCF and the caudal SMF proportional. Free spectrum range (FSR) difference between the HCF cavity and the caudal SMF cavity determines whether the sensitivity is positive or negative. Moreover, temperature sensitivity can be enlarged by reducing the FSR difference, which has a significant guiding role on improving the sensor's sensitivity.

## 2 Sensor Structure and Operate Principle

The CFPIs sensors are fabricated by splicing a segment of HCF between the lead-in SMF and a section of the caudal SMF, as shown in Fig. 1. There are three reflectors in this sensor, namely mirror1 ( $M_1$ ), mirror2 ( $M_2$ ) and mirror3 ( $M_3$ ), respectively. These three mirrors divide the configuration to two mainly FPIs. FPI1 is formed by  $M_1$  and  $M_2$ , whose length marked as  $L_1$ . And FPI2 is formed by  $M_2$  and  $M_3$  and the length of it marked as  $L_2$ . Obviously, these two FPIs are cascaded.

We suppose the reflection coefficient of  $M_1$ ,  $M_2$  and  $M_3$  is  $R_1$ ,  $R_2$  and  $R_3$ .  $n_1$  and  $n_2$  are the effective refractive index of medium in FPI1 and FPI2, correspondingly. When the light propagates to FPI1 and FPI2, the reflection spectra gathered in the lead-in SMF detected are calculated as follows [6]:

$$I_{rr} = \left( \frac{E_r}{E_{in}} \right)^2 = M + N + C + 2\sqrt{MC} \cos(2(\varphi_1 + \varphi_2)) + 2\sqrt{MN} \cos(2\varphi_1) + 2\sqrt{NC} \cos(2\varphi_2) \quad (1)$$

where  $E_{in}$  and  $E_r$  are the input electric field and reflected field, respectively.  $M = R_1$ ,  $N = (1 - R_1)^2 R_2$ ,  $\varphi_1 = 2\pi n_1 L_1 / \lambda$ .  $\varphi_1$  is the phase deviation produced by the FPI1. Wavelength of light is  $\lambda$ .  $P = (1 - R_1)R_2$ ,  $Q = (1 - R_1)R_2^2(1 - R_3)$ ,

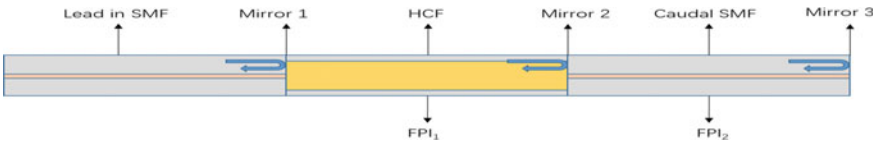


**Fig. 1** Schematic configuration of the present CFPIs optical sensor

$\varphi_2 = 2\pi n_2 L_2 / \lambda$ .  $\varphi_2$  is the phase deviation produced by the FPI2. Where  $C = (1 - R_1)^2(1 - R_2)^2 R_3$ . FSR of the FPI1 and the FPI2 are calculated as [11]

$$\text{FSR}_1 = \frac{\lambda^2}{2n_1 L_1} \quad (2)$$

$$\text{FSR}_2 = \frac{\lambda^2}{2n_2 L_2} \quad (3)$$

For convenience,  $D$  is defined as the difference between FSR1 and FSR2.

$$D = \text{FSR}_1 - \text{FSR}_2 \quad (4)$$

In simulation, we set the length of the air cavity and the quartz cavity properly to guarantee  $D$  very small, which will produce a Vernier effect. The temperature sensitivity of the envelop is calculated as [4]

$$S_{T-\text{envelop}} = \lambda_N \left( \frac{\partial L_2}{\partial T} \frac{1}{L_2} + \frac{\partial n_2}{\partial T} \frac{1}{n_2} \right) \frac{\text{FSR}_1}{\text{FSR}_1 - \text{FSR}_2} \quad (5)$$

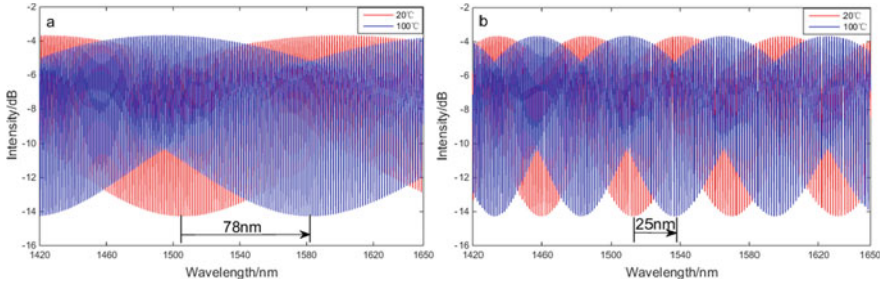
where  $N$  is the resonant order belonging to integer.  $\frac{\partial L_1}{\partial T} \frac{1}{L_1}$  is the thermal expansion coefficient of the HCF, namely the thermal expansion coefficient of the quartz. So  $\frac{\partial L_1}{\partial T} \frac{1}{L_1} = \frac{\partial L_2}{\partial T} \frac{1}{L_2} \cdot \frac{\partial n_1}{\partial T} \frac{1}{n_1}, \frac{\partial n_2}{\partial T} \frac{1}{n_2}$  are the thermo-optical coefficient of the air and the quartz.

### 3 Simulation and Result

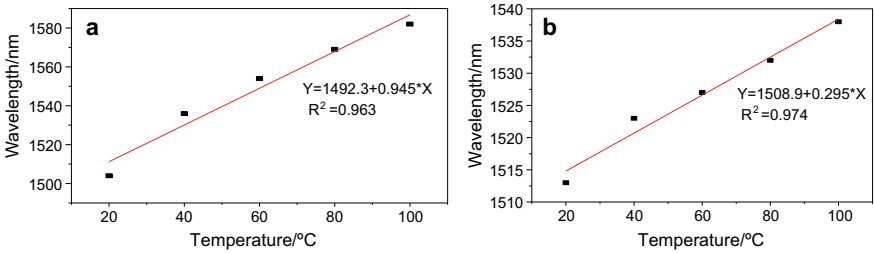
In simulation, we set  $n_1 = 1, n_2 = 1.44, R_1 = R_2 = R_3 = 0.18, \frac{\partial L_1}{\partial T} \frac{1}{L_1} = \frac{\partial L_2}{\partial T} \frac{1}{L_2} = 5.5 \times 10^{-7}/^\circ\text{C}, \frac{\partial n_1}{\partial T} \frac{1}{n_1} = -5.6 \times 10^{-7}/^\circ\text{C}, \frac{\partial n_2}{\partial T} \frac{1}{n_2} = 5.5 \times 10^{-6}/^\circ\text{C}$ . Firstly, we simulate the spectral characteristics of CFPIs sensors under the condition that  $D < 0$  and temperature at 20 and 100 °C.

Figure 2 shows the interference spectra of the CFPIs temperature sensors with  $D < 0$ . Red curves represent the interference spectra at 20 °C. Blue curves show the interference spectra at 100 °C. Figure 2a shows the interference spectra when  $D$  is 0.0119 nm. The FSR of the interference spectra envelops is ~126 nm. Figure 2b shows the interference spectra when  $D$  is 0.0381 nm. The FSR of these envelops is ~39.65 nm. With temperature varying from 20 to 100 °C, because of thermal expansion effect and thermo-optic effect, the interference spectrum in Fig. 2a, b shifts to longer wavelength about 78 nm and 25 nm, respectively.

Figure 3 shows the relationship between the wavelength and temperature within the CFPIs sensors with  $D > 0$ . Figure 3a, b are matched with Fig. 2a, b, respectively. The sensitivity of which are 0.945 nm/°C and 0.295 nm/°C, respectively. Obviously,



**Fig. 2** Interference spectra of the CFPIs temperature sensors with  $D > 0$ . **a**  $L1 = 800 \mu\text{m}$ ,  $L2 = 560 \mu\text{m}$ ,  $D = 0.0119 \text{ nm}$ , **b**  $L1 = 800 \mu\text{m}$ ,  $L2 = 570 \mu\text{m}$ ,  $D = 0.0381 \text{ nm}$



**Fig. 3** Relationship between the wavelength and temperature within the CFPIs temperature sensors with  $D > 0$ . **a**  $L1 = 800 \mu\text{m}$ ,  $L2 = 560 \mu\text{m}$ ,  $D = 0.0119 \text{ nm}$ , **b**  $L1 = 800 \mu\text{m}$ ,  $L2 = 570 \mu\text{m}$ ,  $D = 0.0381 \text{ nm}$

the temperature sensitivity of the sensor where  $D$  is small is larger than that  $D$  is higher. Then, we simulate the spectral characteristics of the CFPIs sensors under the condition that  $D > 0$  and temperature at 20 and 100 °C.

Figure 4 shows the interference spectra of the CFPIs temperature sensors with  $D < 0$ . Red curves represent the interference spectra at 20 °C. Blue curves show the interference spectra at 100 °C. Figure 4a shows the interference spectra

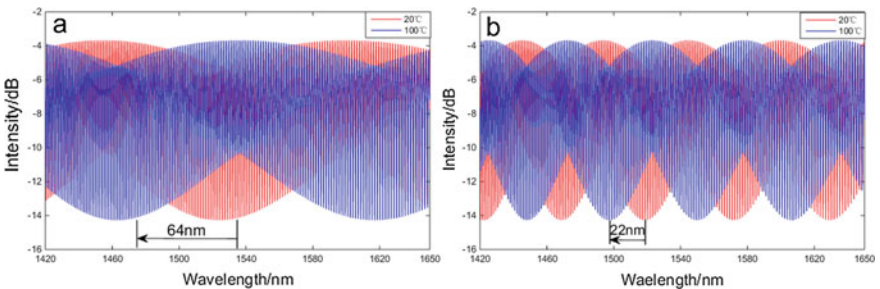
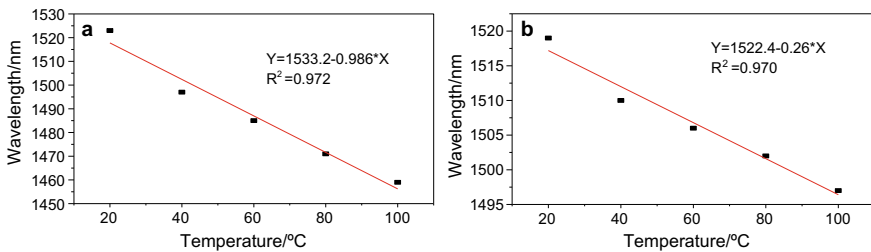


**Fig. 4** Interference spectra of the CFPIs temperature sensors with  $D < 0$ . **a**  $L1 = 800 \mu\text{m}$ ,  $L2 = 550 \mu\text{m}$ ,  $D = -0.0151 \text{ nm}$ , **b**  $L1 = 800 \mu\text{m}$ ,  $L2 = 540 \mu\text{m}$ ,  $D = -0.0433 \text{ nm}$

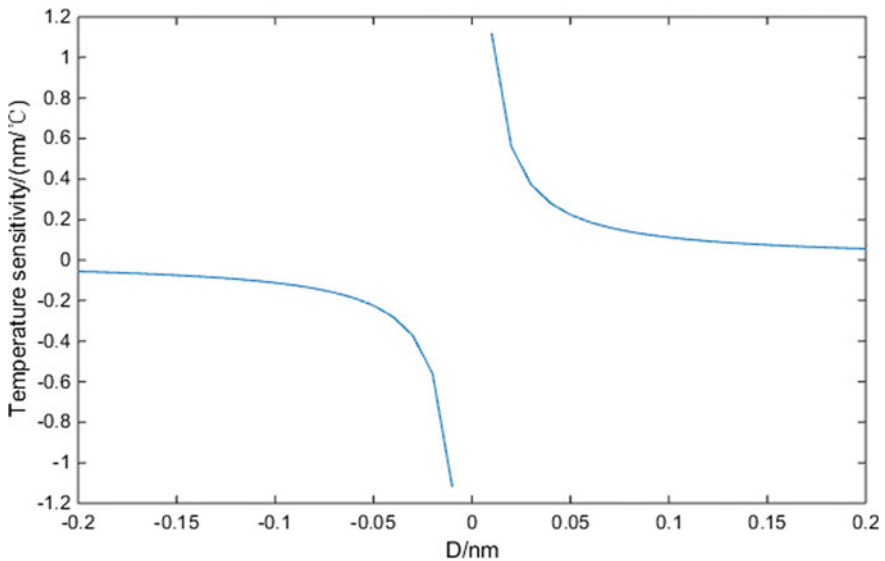
when  $D$  is  $-0.0151$  nm. Figure 2b shows the interference spectra when  $D$  is  $-0.0433$  nm. With temperature varying from 20 to 100 °C, the interference spectra in Fig. 4a, b shift to shorter wavelength about 64 nm and 22 nm, respectively.

Figure 5 shows the relationship between the wavelength and temperature within the CFPIs sensors with  $D < 0$ . Figure 5a, b are matched with Fig. 4a, b, respectively. The temperature sensitivities of them are  $-986$  pm/°C and  $-0.26$  pm/°C. The linear fitting coefficients are up to 0.972 and 0.970, respectively.

As shown in Fig. 6, temperature sensitivity improves with  $|D|$  decreasing. Besides, we can get that when  $D > 0$ , the temperature sensitivity is positive; moreover, the temperature sensitivity will be negative when  $D < 0$ . So a method for controlling



**Fig. 5** Relationship between the wavelength and temperature within the CFPIs temperature sensors with  $D < 0$ . **a**  $L1 = 800 \mu\text{m}$ ,  $L2 = 560 \mu\text{m}$ ,  $D = 0.0119$  nm. **b**  $L1 = 800 \mu\text{m}$ ,  $L2 = 570 \mu\text{m}$ ,  $D = 0.0381$  nm



**Fig. 6** Relationship between the temperature sensitivity and  $D$  value

sensitivity of FPI sensors based on Vernier effect is proposed: adjusting the length of the HCF and the caudal SMF to get higher sensing sensitivity.

## 4 Conclusion

In this paper, we propose a method for controlling the sensitivity of FPI sensors based on Vernier effect. We specially simulate the CFPIs sensors consist of a segment of hollow core fiber (HCF) sandwiched between the lead-in SMF and a section of caudal SMF. Simulation results show that the sensitivity has direct relationship with  $D$ . The interference spectra drift toward longer wavelength and sensitivity are positive when  $D > 0$ . Conversely, the interference spectra drift in the direction of shorter wavelength and the sensitivity are negative when  $D < 0$ . Besides, sensitivity increases with the reduction of  $|D|$ . Therefore, the sensitivity of FPI sensors based on Vernier effect can be controlled by adjusting the length of HCF and SMF, which has a significant guiding role on improving the sensor's sensitivity.

**Funding** This work is funded by Project of The National Key Research and Development Program of China No. 2017YFC0805905 and No. 2018YFF0215104, Project of Natural Science Foundation of China, NSFC (Number: 61775202), the Natural Science Foundation of Zhejiang Province China under Grant No. LY17F050010, National Natural Science Foundation of China (11874332) and National major scientific research instrument development project of Natural Science Foundation of China (61727816).

## References

1. Zhu J et al (2017) An optical fiber Fabry-Perot pressure sensor using corrugated diaphragm and angle polished fiber. *Opt Fiber Technol* 34:42–46
2. Ran Z et al (2015) Novel high-temperature fiber-optic pressure sensor based on etched PCF F-P interferometer micromachined by a 157-nm laser. *IEEE Sens J* 15(7):3955–3958
3. Coutant O, De Mengin M, Le Coarer E (2015) Fabry-Perot optical fiber strainmeter with an embeddable, low-power interrogation system. *Optica* 2(5):400
4. Li Y et al (2018) Optical cascaded Fabry-Perot interferometer hydrogen sensor based on vernier effect. *Opt Commun* 414:166–171
5. Chen P, Shu X, Cao H (2017) Novel compact and low-cost ultraweak Fabry-Perot interferometer as a highly sensitive refractive index sensor. *IEEE Photonics J* 9(5):1–10
6. Tian J, Quan M, Yao Y (2015) Ultra-high sensitivity Fabry-Perot interferometer gas refractive index fiber sensor based on photonic crystal fiber and Vernier effect. *Opt Lett* 40(21):4891
7. Liao H et al (2017) Sensitivity amplification of fiber-optic in-line Mach-Zehnder interferometer sensors with modified Vernier-effect. *Opt Express* 25(22):26898
8. Shao L et al (2015) Sensitivity-enhanced temperature sensor with cascaded fiber optic Sagnac interferometers based on Vernier-effect. *Opt Commun* 336:73–76
9. Zhang P et al (2014) Cascaded fiber-optic Fabry-Perot interferometers with Vernier effect for highly sensitive measurement of axial strain and magnetic field. *Opt Express* 22(16):19581

10. Zhao Y et al (2016) Highly sensitive airflow sensor based on Fabry-Perot interferometer and vernier effect. *J Lightw Technol* 34(23):5351–5356
11. Jiang J et al (2017) Sensitivity-enhanced temperature sensor by hybrid cascaded configuration of a Sagnac loop and a F-P cavity. *Opt Express* 25(26):33290